ELSEVIER

Catalysis Today 50 (1999) 125–132

CATALYSIS TODAY

Numerical modeling of the reduction of nitric oxide by ethylene over Cu-ZSM-5 under lean conditions

Ronald A. Wilber, André L. Boehman*

Fuel Science Program, Department of Materials Science and Engineering, The Pennsylvania State University, University Park, PA 16802, USA

Abstract

Some catalysts such as copper zeolites have shown promise for direct NO decomposition and selective NO reduction via hydrocarbons in lean exhausts. This paper describes modeling calculations for the performance of a Cu-ZSM-5 NO_x reduction catalyst. The numerical model simulates the multi-component transport and reaction processes that occur within a catalyzed monolith support. The surface boundary conditions for the reacting species are satisfied through the use of multi-dimensional Newton–Raphson iteration. The model is used to formulate global rate expressions for the oxidation of C_2H_4 and the reduction of NO by adjusting kinetic parameters until predicted conversion efficiencies match experimental data. Results from simulation of NO reduction by C_2H_4 are compared to previous simulation of NO reduction by C_3H_6 and provide a detailed explanation of the differences between the efficiency of C_2H_4 and C_3H_6 as reductants. Then the numerical model is compared to data from higher space velocities to test the validity of the kinetic model. The comparison shows that additional optimization of the kinetic parameters is required. Nonetheless, the simulated interactions within the catalytic passage demonstrate important features of selective NO reduction.

Keywords: NO_x; Selective catalytic reduction; Diesel; Zeolite; Modeling; Cu-ZSM-5

1. Introduction

The growing need for a NO_x reduction catalyst for diesel engines has prompted a worldwide search for a ''lean NO_x catalyst''. At present, the approach for reducing NO_x in lean exhausts showing the most commercial potential involves precious metal catalysts and injection of a supplemental reductant into the exhaust system [1]. The need for a supplemental reductant is due to the low concentration of unburned hydrocarbons in typical diesel exhausts. Some reductants that have been considered include ethanol [1], diesel fuel [1], and urea [2]. Problems common to these precious metal based catalysts are poor selectivity to N_2, i.e., excessive N_2O formation, a narrow temperature range for maximum catalytic activity, and poor hydrocarbon selectivity, i.e., the hydrocarbon reductant oxidizes more rapidly than it reduces NO.

In contrast, zeolites, particularly Cu-ZSM-5, have demonstrated an ability to stoichiometrically reduce NO to N_2 and O_2 [3]. However, as is commonly known, the Cu-ZSM-5 catalyst loses activity rapidly in the presence of water vapor and sulfur, so this catalyst is not presently commercially viable. Nonetheless, Cu-ZSM-5 exhibits an intriguing ability to directly decompose NO and to reduce NO with a hydrocarbon reductant. In the work of Cho [4], an

*Corresponding author. Tel.: +1-814-865-7839; fax: +1-814-865-3075; e-mail: boehman@ems.psu.edu

0920-5861/99/$ – see front matter
PII: S0920-5861(98)00469-6

interesting comparison is made between the efficacy of different hydrocarbons as reductants over Cu-ZSM-5. While C_3H_6 displays a lower activation energy and light-off temperature than C_2H_4, C_2H_4 proves to be the more effective reductant for NO. When both C_2H_4 and C_3H_6 were present as reductants, Cho observed a ''kinetic antagonism'' between the two hydrocarbons over Cu-ZSM-5. There are two explanations, perhaps closely related, for the observed difference in ability to reduce NO. One explanation is that, for reasons of a physical chemistry nature, C_2H_4 is a more selective reductant, e.g., the structure of the adsorbed hydrocarbon molecule and the intermediate species that it may form. The other explanation is based on the simple fact that less C_3H_6 remained available to react with NO on the zeolite surface because of its greater oxidation activity. Consequently, C_2H_4 may not have any more affinity for reaction with NO than C_3H_6, but may have instead remained available to react with NO due to its slower oxidation rate. Cho also points out that C_2H_4 may be the more relevant hydrocarbon to study because it is present in higher concentrations than C_3H_6 in vehicle exhausts. In typical gasoline engine exhaust, the ratio of the concentration of ethylene to propylene is about 3:1, and in diesel engines this ratio is slightly larger [4].

In the present work, we have extended a model previously applied to the C_3H_6+NO+O_2 reaction system [5], to the study of the C_2H_4+NO+O_2 reaction system. Here we provide a brief overview of the numerical method, present a comparison of simulation results and the experimental measurements of Cho [4], and present a comparison of the C_3H_6+NO+O_2 and C_2H_4+NO+O_2 reaction systems. The intent of this work is to gain an understanding and an ability to simulate the competitive reactions taking place over Cu-ZSM-5 during lean NO_x reduction.

2. Numerical

Fig. 1 shows the mathematical representation of the monolith supported Cu-ZSM-5 catalyst used as the basis for the numerical model. The rectangular passages of the monolith have been reduced to a single, cylindrical, isothermal passage. The inevitable filleting of the corners in the square monolith cell results in the assumption of a cylindrical passage. The walls of the passage are assumed isothermal so that only convective transport and transverse diffusion of species are considered. Flow in the passage is assumed to be fully developed throughout. Surface reactions are assumed to be adequately described as apparent or overall rates given by global kinetic rate laws. More detail on the numerical approach is provided elsewhere [5]. Table 1 presents geometric and flow conditions used in these simulations which are based on the experiments of Cho [4].

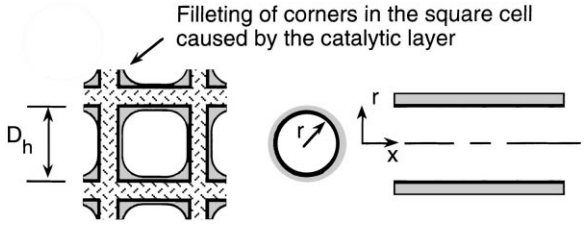

Fig. 1. Cylindrical representation of the square monolith cell.

The two reactions of interest here are the oxidation of ethylene, Eq. (1), and the reduction of nitric oxide by ethylene, Eq. (2):

$$C_2H_4 + 3O_2 \rightarrow 2CO_2 + 2H_2O \quad (1)$$

$$NO + \tfrac{1}{6}C_2H_4 \rightarrow \tfrac{1}{3}CO_2 + \tfrac{1}{3}H_2O + \tfrac{1}{2}N_2 \quad (2)$$

The numerical model solves the species transport equation for each species considered, C_2H_4, NO, O_2, CO_2, H_2O, and N_2, given by

$$\rho u \frac{\partial y_i}{\partial z} - \rho D_{im} \frac{1}{r}\frac{\partial}{\partial r}\left(r\frac{\partial y_i}{\partial r}\right) = 0 \quad (3)$$

while satisfying a coupled non-linear boundary condition at the catalyst surface:

$$-\rho D_{im}\frac{\partial y_i}{\partial r} = \sum_{k=1}^{NRXN} \dot{R}_k f_{i,k}, \quad (4)$$

where ρ is the mixture averaged density, D_{im} the bulk

Table 1
Geometric and flow conditions

Parameter	Value or range
Re_D	0.26–0.33, 0.7–0.96
Space velocity (h^{-1})	12 000, 35 000
D_h (cm)	0.1017
L (cm)	2.5

diffusion coefficient for species i, y_i the mass fraction of species i, u the axial velocity, z the axial coordinate, r the radial coordinate, *NRXN* the number of reactions to be considered at the catalytic surface (2, in this case), $\dot{R}_k$ the rate of reaction k, and $f_{i,k}$ is the mass action coefficient for species i. The framework for representing the two reactions of interest is as follows. Each reactant can be assigned to be a primary reactant, i.e., a species for which a chemical balance equation describes the mechanism for the removal of that species and for which that removal rate will be quantified via a rate law. Other reactants can be consumed, but only the consumption of the primary reactants is directly calculated. Conversion of the other reactants and production of the product species are inferred from the reaction rates of the primary reactants. For each reaction, mass action coefficients define the rate of consumption or production of each species, and for each reaction, the mass action coefficients have been normalized based on one of the primary reactants. In this case, Eq. (1) is normalized on C_2H_4 and Eq. (2) is normalized on NO. For the primary reactants, Eq. (4) represents a coupled boundary condition that must be satisfied in concert with the conservation equations via iteration. The scheme used here is multi-dimensional Newton–Raphson, based on routines MNEWT, LUDCMP and LUBKSB from Numerical Recipes [6]. The iteration scheme requires that the user defines a Jacobian, or sensitivity coefficient matrix, along with a vector containing the values of the function whose zeros are to be found. The function is given by

$$F_i = \rho D_{im} \frac{\partial y_i}{\partial r} + \sum_{k=1}^{NRXN} \dot{R}_k f_{i,k} \tag{5}$$

and the matrix (of dimensions *NRXN*×*NRXN*) and vector (of length *NRXN*) are given by

$$\beta_i = -F_i, \tag{6}$$

$$\alpha_{ij} = \frac{\partial F_i}{\partial y_j}. \tag{7}$$

The multi-dimensional Newton–Raphson scheme then calculates the adjustments to make to the iterates (in this case, the surface concentrations of NO and C_2H_4), by finding the solution to the system of equations defined by

$$\alpha_{ij}\,\Delta y_j = \beta_i, \tag{8}$$

where Δy_j is the vector adjustments to the surface concentration of each primary reactant.

Eq. (3) is solved by a finite difference approach using second order backward differencing for the advection term and second order central differencing for the diffusion term. A diagonal matrix results from this implicit differencing scheme. A pentadiagonal matrix inversion is performed, so that second order backward differences can be used to describe the gradients at the centerline of the catalytic passage and at the catalytic surface. Since Eq. (4) must be solved at every axial location in the computational domain, the marching scheme for advancing the species conservation equations involves iterating on Eq. (5) until all entries in the function F_i are smaller than 1×10^{-6}. Typically, the solution at each axial location required anywhere from 20 to 300 iterations to reach convergence. All simulations were performed on a 100 MHz Pentium personal computer.

3. Kinetic model

The kinetic model for the heterogeneous reaction of C_2H_4 and NO over Cu-ZSM-5 was assumed to follow a Langmuir–Hinshelwood dual site mechanism [7]. For the oxidation of C_2H_4, the rate law form was based on the form originally suggested by Voltz et al. [8] and later updated by Oh and Cavendish [9]. For the reduction of NO by C_2H_4, the rate law was based on the form suggested by Cho [4]. In these global rate expressions, A_I are pre-exponential factors and E_I are either activation energies or equilibrium adsorption energies, depending on whether they occur in the driving force for reaction (numerator) or in the inhibition term (denominator):

$$\dot{R}_{C_2H_4} = \frac{A_1 \chi_{C_2H_4} \chi_{O_2}\, e^{-E_1/RT}}{G}, \tag{9}$$

where

$$G = T[1 + 65.5\chi_{C_2H_4}\, e^{E_2/RT}]^2 \times [1 + 4.79\times10^5 \chi_{NO}^{0.7}\, e^{-3733/T}],$$

$$\dot{R}_{NO} = \frac{A_2 \chi_{NO} \chi_{C_2H_4} e^{(-E_3/RT)}}{[T^n(1 + A_3\chi_{NO} e^{(-E_4/RT)^2}]}. \tag{10}$$

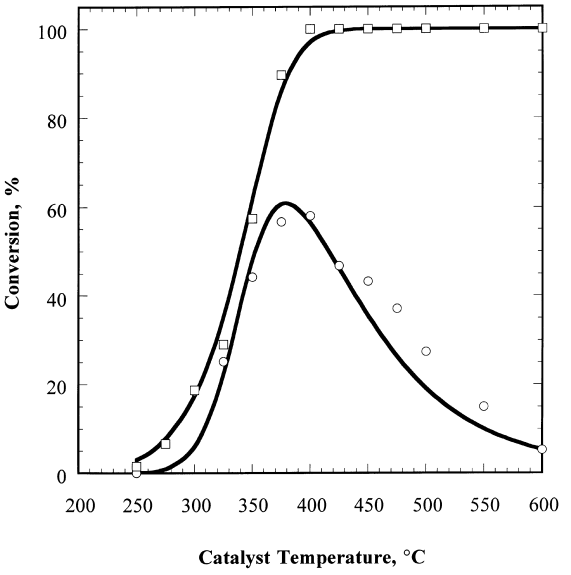

Fig. 2. Conversion efficiency versus catalyst temperature for C_2H_4 (□) and NO (○). Flow conditions of 1200 ppm C_2H_4, 230 ppm NO, 7% O_2, balance He. Comparison between numerical simulations and the experimental data of Cho [4] at 12 000 h^{-1} space velocity.

4. Results and discussion

The application of the numerical model to the experimental data of Cho [4] for a space velocity of 12 000 h^{-1} yielded the comparison shown in Fig. 2, after a manual ''trial and error'' optimization of some kinetic parameters. Primary attention was focused on reproducing the critical trends of the catalyst's light-off behavior, specifically that the NO reduction and C_2H_4 oxidation reactions begin to increase sharply at about the same temperature; and that the NO reduction reaction reaches a maximum and falls off to zero activity at higher temperatures. These trends are captured by the kinetic model using the values of the kinetic parameters shown in Table 2. The results in Fig. 2 represent a sequence of separate simulations of the monolith passage. At more than a dozen values of catalyst inlet temperature, the numerical model simulated the flow and reactions along the monolith. The overall conversion efficiency for C_2H_4 and NO are computed during each simulation and the results are compiled in the figure. Fig. 3 shows the comparison between the experimental conversion efficiencies from Cho [4] and the simulation results [5] for the

Table 2
Final kinetic parameter values for the C_2H_4+NO+O_2 reaction system

Parameter	Final value
A_1	0.238×10^{10} g C_2H_4–K/cm^2 s
A_2	0.625×10^{4} g NO–K$^{1.5}$/cm^2 s
A_3	1×10^{-6}
E_1/R	12 500 K
E_2/R	−961 K
E_3/R	0.0
E_4/R	−14 050 K
n	1.5

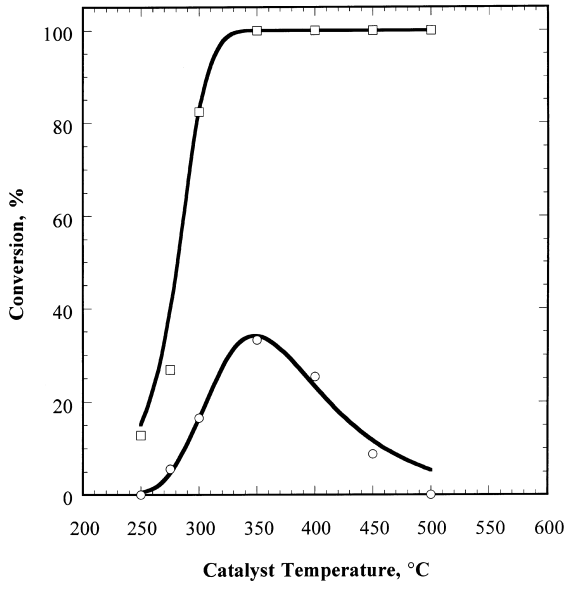

Fig. 3. Conversion efficiency versus catalyst temperature for C_3H_6 (□) and NO (○). Flow conditions of 800 ppm C_3H_6, 230 ppm NO, 7% O_2, balance He. Comparison between numerical simulations and the experimental data of Cho [4] at 12 000 h^{-1} space velocity.

C_3H_6+NO+O_2 reaction system. Please note that the data presented here for the C_3H_6+NO+O_2 reaction system are from new simulation results that have corrected a mistake in [5]. Updated kinetic parameters for the C_3H_6+NO+O_2 reaction system are presented in Table 3. The only change is that the factors A_1 and A_2 have been decreased by a factor of 4 from the results in [5]. The trends shown in Fig. 3 are nearly identical to those presented in [5]. Comparison of Figs. 2 and 3 clearly shows the differences between the behavior of C_3H_6 and C_2H_4 as reductant for lean

Table 3
Updated kinetic parameter values for the C_3H_6+NO+O_2 reaction system

Parameter	Final value
A_1	1.28×10^{10} g C_3H_6–K/cm^2 s
A_2	0.113×10^{4} g NO–K$^{1.5}$/cm^2 s
A_3	1×10^{-6}
E_1/R	11 000 K
E_2/R	−500 K
E_3/R	0.0
E_4/R	−13 500 K
n	1.5

NO conversion. In contrast to the C_3H_6+NO+O_2 reaction system, C_2H_4 remains available to react with the NO at higher temperatures because the oxidation reaction for C_2H_4 is less active than for C_3H_6. The higher availability of C_2H_4 to participate in the reduction reaction at higher temperatures leads to higher observed conversion efficiencies (58% for C_2H_4 at 400°C versus 33% for C_3H_6 at 350°C) [4], which are reproduced in these simulations.

Figs. 2 and 3 present the overall conversions at the end of the 2.5 cm long monolith cell obtained from numerous solutions of the catalytic passage model, each for a different value of catalyst temperature. Examination of the predicted behavior within the passageways of the monolith reactor is also instructive for understanding the competing oxidation and reduction reactions and for understanding how the differences between C_3H_6 and C_2H_4 are manifested. Within each passageway of the monolith, the surface and bulk concentrations vary with axial distance. Fig. 4 shows the axial variation of normalized surface concentration (normalized against the inlet concentrations) of NO and C_2H_4 for three of the simulations at 300°C, 350°C and 400°C. Fig. 5 shows the axial variation of normalized surface concentration of NO and C_3H_6 for three of the simulations at 300°C, 350°C and 400°C. For the C_2H_4+NO+O_2 reaction system and catalyst inlet temperatures below 350°C, the surface concentrations of C_2H_4 and NO vary gradually with axial distance, and the oxidation and reduction reactions proceed at rates controlled by the species concentrations and the catalyst temperature. For inlet temperatures above about 350°C, the C_2H_4 oxidation reaction transitions to diffusion control, and consequently, the

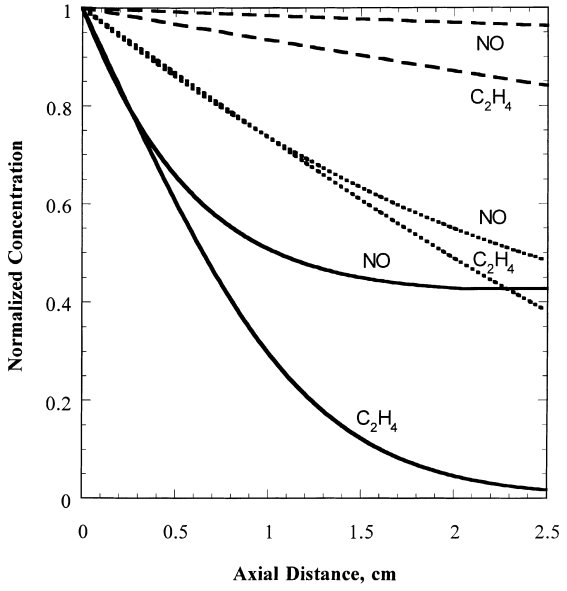

Fig. 4. Normalized surface concentration of C_2H_4 and NO versus axial distance in a catalytic passage at catalyst temperatures of 300°C (- - -), 350°C (· · ·) and 400°C (———). Flow conditions of 1200 ppm C_2H_4, 230 ppm NO, 7% O_2, balance He. Numerical simulations based on the experimental data of Cho [4] at 12 000 h^{-1} space velocity.

NO reduction reaction ceases. For the C_3H_6+NO+O_2 reaction system, this transition from kinetically limited to diffusion limited oxidation occurs at a much lower temperature of 300°C. At the highest temperatures shown in Figs. 4 and 5 (400°C), the NO reduction reaction progresses at a higher rate than at the intermediate temperature shown, but the net NO conversion is lower because at elevated temperature, the reductant becomes rapidly depleted. Fig. 6 presents a comparison of the normalized surface concentrations for the two reaction systems at a catalyst inlet temperature of 375°C. This plot clearly shows why C_2H_4 is a more effective reductant than C_3H_6, despite the higher oxidation activity of C_3H_6. Although the predicted NO reaction rate is initially higher at 375°C for C_3H_6, the rapid depletion of C_3H_6 by oxidation causes the NO reduction reaction to shut down near the inlet of the monolith passage. However, C_2H_4 remains on the catalyst surface throughout the passage allowing the reduction reaction, which is activated at this temperature, to progress much farther than for the C_3H_6+NO+O_2 reaction system.

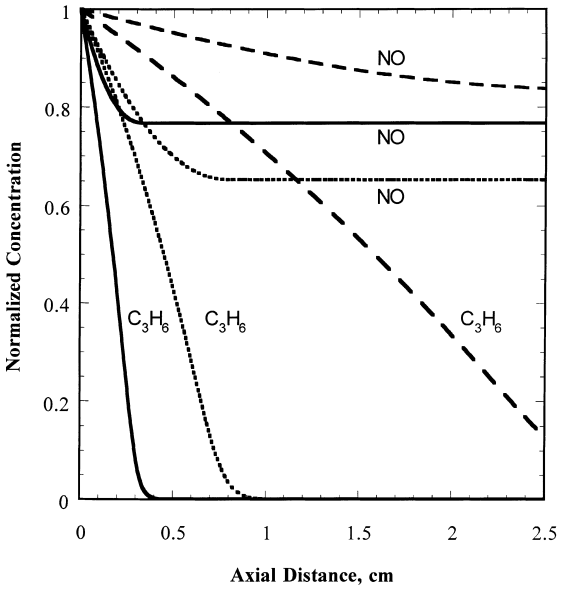

Fig. 5. Normalized surface concentration of C_3H_6 and NO versus axial distance in a catalytic passage at catalyst temperatures of 300°C (- - -), 350°C (· · ·) and 400°C (———). Flow conditions of 800 ppm C_3H_6, 230 ppm NO, 7% O_2, balance He. Numerical simulations based on the experimental data of Cho [4] at 12 000 h^{-1} space velocity.

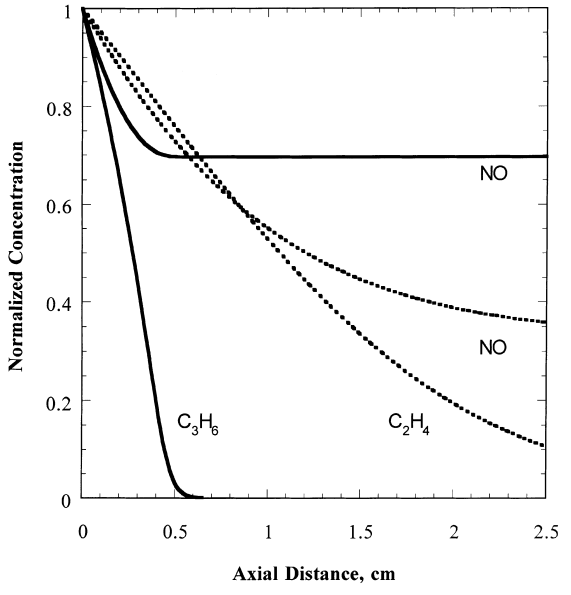

Fig. 6. Normalized surface concentrations of C_2H_4, C_3H_6 and NO versus axial distance at catalyst temperatures of 375°C for the C_2H_4+NO+O_2 reaction system (· · ·) and C_3H_6+NO+O_2 reaction system (———). Flow conditions as in Figs. 4 and 5, respectively.

The test of the kinetic model is how well it can be extrapolated to other experimental conditions. Verification of the kinetic model was obtained by application of the numerical model to another of Cho's test conditions. At a space velocity of 35 000 h^{-1}, the kinetic model provides poor agreement between prediction and experiment for NO reduction. As shown in Fig. 7, the model qualitatively predicts the oxidation and reduction behavior by matching the trend with reaction temperature, but the peak NO conversion is not correctly reproduced. As shown in Fig. 8, the simulation of the C_3H_6+NO+O_2 reaction system provided better agreement with experiment for the higher space velocity. Nonetheless, at both space velocities the trends observed in Cho's experiments for NO reduction by C_2H_4 over Cu-ZSM-5 can be predicted reasonably well by the present model. Further optimization of the kinetic parameters will be possible when the determination of kinetic parameters is performed by a numerical optimization scheme instead of by the manual "trial and error" method used here.

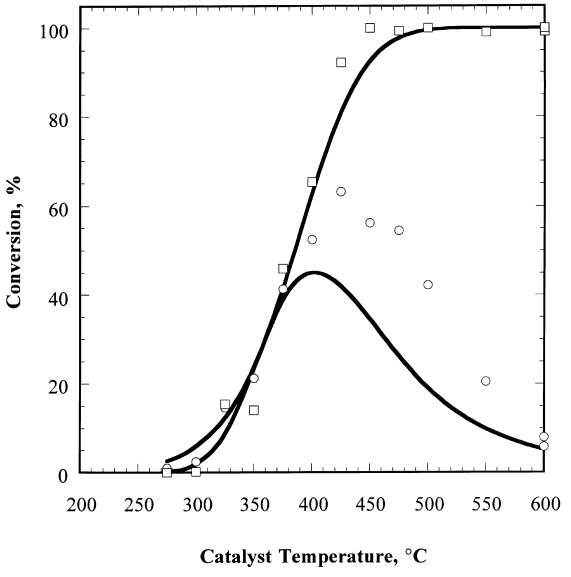

Fig. 7. Conversion efficiency versus catalyst temperature for C_2H_4 (□) and NO (○). Flow conditions of 1200 ppm C_2H_4, 230 ppm NO, 7% O_2, balance He. Comparison between numerical simulations and the experimental data of Cho [4] at 35 000 h^{-1} space velocity.

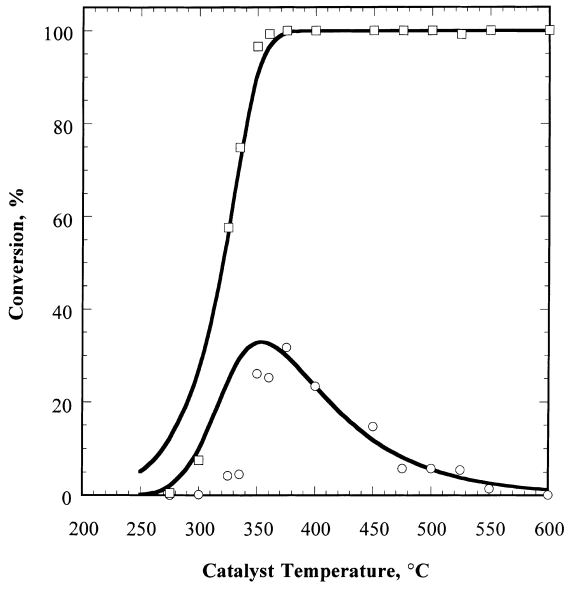

Fig. 8. Conversion efficiency versus catalyst temperature for C_3H_6 (□) and NO (○). Flow conditions of 800 ppm C_3H_6, 230 ppm NO, 7% O_2, balance He. Comparison between numerical simulations and the experimental data of Cho [4] at 35 000 h^{-1} space velocity.

As postulated by Cho [4] and confirmed experimentally by Cho [10], and supported by Burch and coworkers [11,12], the mechanism of lean NO conversion by hydrocarbons (specifically by C_2H_4 and C_3H_6) involves dissociation of NO on catalyst sites reduced by the hydrocarbon reductant. The nitrogen atoms combine and desorb as N_2, while the oxygen remains adsorbed until it is ''cleaned-off'' the surface by the hydrocarbon [10,11]. This mechanism, which appears to be supported by both steady state [4,10] and transient [10] experiments, may explain the observed differences between C_2H_4 and C_3H_6 as reductants. If the sole function of the reductant is to maintain active centers in the reduced state for dissociative adsorption of NO, then the reductant with a higher oxidation activity should provide greater NO conversion. However, for C_3H_6 the rapid onset of oxidation leading to catalyst light-off occurs at a temperature that is lower than the active range of the NO conversion reaction. So, while C_3H_6 can scavenge oxygen from the catalyst sites, it rapidly becomes depleted at temperatures where high rates of NO conversion can occur. The NO conversion activity of C_2H_4 arises because C_2H_4 continues to scavenge oxygen well into the temperature range where rapid NO conversion occurs.

Adams et al. [13] have examined the influence of space velocity on the behavior of Cu-ZSM-5. They also report, as did Bennett et al. [14], activation energy and pre-exponential factors determined for NO reduction by C_3H_6, assuming first order reaction. A comparison of kinetic parameters reported by Adams et al. with the present results shows some agreement for the activation energy of the C_3H_6 oxidation reaction (19±3 kcal/mol [13] versus 22 kcal/mol) but no agreement for the NO reduction reaction (15±3 kcal/mol [13] versus 27 kcal/mol). However, the trends Adams et al. observed with space velocity are consistent with the observations of Cho [4] and the predictions of the present model.

5. Conclusions

The behavior of the C_2H_4+NO+O_2 reaction system has been simulated successfully by the present numerical approach. The critical trend, a narrow temperature window within which NO conversion reaches a maximum level and then falls off sharply, has been reproduced by fitting kinetic parameters in a global expression for the overall rates of C_2H_4 oxidation and NO reduction. Further optimization of the kinetic parameters may provide a more robust description of the NO conversion process, and allow extrapolation to diverse reaction conditions. At present, further optimization of the kinetic parameters is needed. Comparison of the simulations for the C_2H_4+NO+O_2 and C_3H_6+NO+O_2 reaction systems provides a detailed explanation for the higher observed NO reduction efficiency of C_2H_4. Because C_2H_4 oxidizes more slowly than C_3H_6, it remains available to react with NO at temperatures where the NO reduction is more rapid. Simulation results at 12 000 h^{-1} space velocity compare well with the experimental results of Cho [4], but agreement degrades when the model is extrapolated to higher space velocity.

6. Nomenclature

A_1 pre-exponential factor in Eq. (9) (g C_2H_4–K/cm^2 s)

A_2 pre-exponential factor in Eq. (10) (g NO–$K^{1.5}$/cm^2 s)
A_3 frequency factor in Eq. (10)
D_h hydraulic diameter (cm)
D_{im} bulk diffusion coefficient for species i (cm/s)
E_1 activation energy in Eq. (9) (J/mol)
E_2 activation energy in Eq. (10) (J/mol)
E_3 activation energy in Eq. (10) (J/mol)
F_i function of defining the balance of reaction and diffusion at the catalytic surface
$f_{i,k}$ mass action coefficient for species i
L length of the monolith (cm)
r radial coordinate (cm)
R ideal gas constant (8.314 J/mol K)
Re_D Reynolds number based on hydraulic diameter
$\dot{R}_k$ rate of reaction for reaction k (g/cm^2 s)
u axial velocity (function of r only) (cm/s)
y_i mass fraction of species i
z axial coordinate (cm)

Greeks

α_{ij} sensitivity coefficient matrix for multi-dimensional Newton–Raphson iteration
β_i vector for multi-dimensional Newton–Raphson iteration
χ_i mole fraction for species i

Acknowledgements

The authors wish to thank Dr. B.K. Cho of the Physical Chemistry Department, General Motors Research and Development Center, for supplying his original experimental results from Ref. [4]. The authors also wish to thank Drs. C. Song, M.T. Klein, B. Johnson and J.G. Reynolds, who organized the 1997 ACS Symposium on Catalysis in Fuel Processing and Environmental Protection held in Las Vegas, 1997.

References

[1] M.J. Heimrich, Society of Automotive Engineers, Paper no. 970755 (1997).
[2] W. Held, A. König, T. Richter, L. Puppe, Society of Automotive Engineers, Paper no. 900496 (1990).
[3] M. Iwamoto, H. Hamada, Catal. Today 10 (1991) 57–71.
[4] B.K. Cho, J. Catal. 142 (1993) 418–429.
[5] A.L. Boehman, Society of Automotive Engineers, Paper no. 970752 (1997).
[6] W.H. Press, B.P. Flannery, S.A. Teukolsky, W.T. Vetterling, Numerical Recipes, University of Cambridge Press, Cambridge, UK, 1986, pp. 269–273.
[7] M. Boudart, G. Djéga-Mariadassou, Kinetics of Heterogeneous Catalytic Reactions, Princeton University Press, Princeton, NJ, 1984, pp. 90–105.
[8] S.E. Voltz, C.R. Morgan, D. Liederman, S.M. Jacob, Ind. Eng. Chem. Prod. Res. Dev. 12 (1973) 294–301.
[9] S.H. Oh, J.C. Cavendish, Ind. Eng. Chem. Prod. Res. Dev. 21 (1982) 29–37.
[10] B.K. Cho, J. Catal. 155 (1995) 184–195.
[11] R. Burch, S. Scire, Appl. Catal. B 3 (1994) 295–318.
[12] R. Burch, P.J. Millington, A.P. Walker, Appl. Catal. B 4 (1994) 65–94.
[13] K.M. Adams, J.V. Cavataio, R.H. Hammerle, Appl. Catal. B 10 (1996) 157–181.
[14] C.J. Bennett, P.S. Bennett, S.E. Golunski, J.W. Hayes, A.P. Walker, Appl. Catal. A 86 (1992) L1–L6.